

Principled and Efficient Transfer Learning of Deep Models via Neural Collapse

Xiao Li^{*#}, Sheng Liu^{*◇}, Jinxin Zhou[†], Xinyu Lu[§], Carlos Fernandez-Granda^{◇,‡}, Zhihui Zhu[†], and Qing Qu[#]

[#]Department of Electrical Engineering and Computer Science, University of Michigan

[◇]Center for Data Science, New York University

[‡]Courant Institute of Mathematical Sciences, New York University

[†]Department of Computer Science & Engineering, Ohio State University

[§]Language Technologies Institute, Carnegie Mellon University

January 5, 2023

Abstract

With the ever-growing model size and the limited availability of labeled training data, transfer learning has become an increasingly popular approach in many science and engineering domains. For classification problems, this work delves into the mystery of transfer learning through an intriguing phenomenon termed neural collapse (NC), where the last-layer features and classifiers of learned deep networks satisfy: (i) the within-class variability of the features collapses to zero, and (ii) the between-class feature means are maximally and equally separated. Through the lens of NC, our findings for transfer learning are the following: (i) when pre-training models, preventing intra-class variability collapse (to a certain extent) better preserves the intrinsic structures of the input data, so that it leads to better model transferability; (ii) when fine-tuning models on downstream tasks, obtaining features with more NC on downstream data results in better test accuracy on the given task. The above results not only demystify many widely used heuristics in model pre-training (e.g., data augmentation, projection head, self-supervised learning), but also leads to more efficient and principled fine-tuning method on downstream tasks that we demonstrate through extensive experimental results.

1 Introduction

Transfer learning has become an increasingly popular approach in computer vision, medical imaging, and natural language processing [1, 2, 3]. With domain similarity, a pre-trained large model on upstream datasets is reused as a starting point or feature extractor for fine-tuning a new model on a much smaller downstream task [1]. The pre-trained model reuse during fine-tuning significantly reduces the computational cost, and achieves superior performances on problems with limited training datasets.

However, without principled guidance, the underlying mechanism of transfer learning is not very well understood. First, when we are pre-training deep models on the upstream dataset, we

^{*}The first two authors contributed equally to the work.

lack good metrics for measuring the quality of the learned model or representation in terms of transferability. In the past, people tended to rely empirically on controversial metrics for predicting the transferred test performance, such as the validation accuracy on the pre-trained data (e.g., validation accuracy on ImageNet [4]). For example, some popular approaches (e.g., label smoothing [5] and dropout [6]) for boosting ImageNet validation accuracy turn out to hurt transfer performance on downstream tasks [7]. Additionally, when pre-training deep models, many heuristic methods improving transferability, such as the design of loss functions, data augmentations, increased model size, and projection head layers [8, 9], are designed largely based upon trial-and-error without much insight of the underlying mechanism. Second, given the pre-trained models, how to efficiently fine-tune the model on downstream tasks remains an open question. Although fully fine-tuning all the parameters of the pre-trained model achieves the best performance, it becomes increasingly expensive as the model size grows (e.g., GPT-3 and transformer [10, 11, 2, 12]). All these challenges call for a deeper understanding of what makes pre-trained deep models more transferable.

In this work, we study the underlying principles of transfer learning based upon an intriguing phenomenon has been recently discovered in terms of the representations, termed *Neural Collapse* (\mathcal{NC}) [13, 14]. Recently, for classification problems, the \mathcal{NC} is an intriguing phenomenon has been discovered in terms of learned deep representations (see Figure 1), in which the last-layer features and classifiers *collapse* to simple but elegant mathematical structures on the training data: (i) for each class, the intra-class variability of last-layer features collapses to zero, and (ii) the between-class class means and the last-layer classifiers all collapse to the vertices of a Simplex Equiangular Tight Frame (ETF) up to scaling. This \mathcal{NC} phenomenon [13, 14] has been empirically demonstrated to persist across a variety of network architectures and datasets. Theoretically, recent works justified the prevalence of \mathcal{NC} under simplified unconstrained feature models across a variety of training losses [15, 16, 17, 18] and problem formulations [19, 20, 21]. However, despite of recent endeavors of demystifying the \mathcal{NC} phenomenon, a fundamental question lingers: *is \mathcal{NC} a blessing or a curse for deep representation learning?* This work address this question in terms of transfer learning.

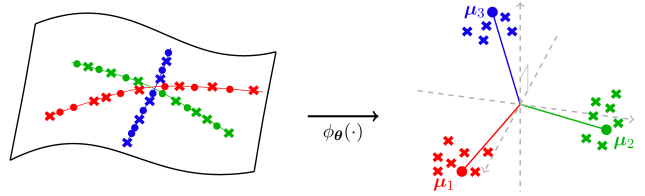


Figure 1: **An illustration of neural collapse.** Here dots \bullet represent training samples, crosses \times stand for the testing samples, and $\phi_\theta(\cdot) : \mathbb{R}^D \rightarrow \mathbb{R}^d$ denotes the feature mapping of the network, i.e., the output of the penultimate layer.

Contributions of this work. In this work, we provide a comprehensive investigation of the relationship between the transferability of pre-trained models and \mathcal{NC} . As \mathcal{NC} implies that intra-class variability for each class collapses to zero, the representations learned via *vanilla* supervised learning fails to capture the intrinsic dimensionality of the input data, and hence they often result in poor performance of transferability. Intuitively, to make the pre-trained models transferable, for each class the learned features should be discriminative but *diverse enough* that they can preserve the intrinsic structures of the input data. On the other hand, on the downstream task when we fine-tune pre-trained models, we desire more collapse of the features on the downstream training data.

Based upon such intuitions, we adapt the metrics for evaluating \mathcal{NC} to measure the quality of learned representations in terms of both *intra-class diversity* and *between-class discrimination*. As such, not only can we universally demystify several heuristics that are widely used in transfer

learning, but it also leads to more principled and efficient fine-tuning methods of large pre-trained models on downstream data. In words, our empirical findings based upon the \mathcal{NC} metrics can be summarized as follows.

- **Less collapsed features on source data leads to better transferability to certain extents.** By evaluating the \mathcal{NC} metrics on different loss functions [22] and several widely used techniques in transfer learning (e.g., the projection head, various data augmentations [8, 23, 9], and adversarial training [24, 25]), we find that the more diverse the features are, the better the transferability of the pre-trained model. In comparison to previous works [26, 7], however, we showed that this only holds to a certain extent as random features are not collapse but they do not generalize well.¹ Moreover, we further use the relationship for explaining the underlying mechanism of many popular heuristics for transfer learning.
- **More collapse of fine-tuned models leads to better test performance on downstream tasks.** In contrast, when we are evaluating different pre-trained models on downstream tasks, we observe that more collapsed features on downstream data usually lead to better transfer accuracy. We demonstrate the universality across a variety of downstream data [27, 28, 29, 30] as well as pre-trained models [31, 12, 32, 33]. Moreover, we further showed that this phenomenon not only happens on the penultimate layer across different pre-trained models, but also across different layers of the same pre-trained model.
- **Pre-trained models can be more effectively fine-tuned through \mathcal{NC} .** Efficient and effective transfer learning is of paramount importance for large models nowadays [34, 35, 36]. Inspired by the above findings, we show that we can design simple but more memory-efficient fine-tuning methods by collapsing the features of the penultimate layer. By experiments on a variety of network architectures, we demonstrate that the proposed fine-tuning strategy achieves on-par or even better performances compared with full model fine-tuning and is also more robust against data scarcity.

Relationship to prior arts. The prevalence of \mathcal{NC} phenomenon has caught significant attention both in practice and theory recently, and our work draws the connection between \mathcal{NC} and transfer learning. On the other hand, a few recent works are investigating the properties of deep representations for transfer learning, which is also related to ours. We’d like to summarize and briefly discuss those results below.

- **Understandings of the \mathcal{NC} phenomenon.** There is a line of recent works deciphering training, generalization, and transferability of deep networks in terms of \mathcal{NC} , that are related to ours (see a recent review work [37]). For training, recent works showed that \mathcal{NC} happens for a variety of loss functions and formulations, such as cross-entropy (CE) [13, 38, 15, 19, 39, 21], mean-squared error (MSE) [40, 14, 17, 20, 41], and supervised contrastive (SupCon) loss [16]. For generalization, the work [42] shows that \mathcal{NC} also happens on test data drawn from the same distribution asymptotically, but not for finite samples [43]. On the other hand, quite a few recent works [13, 42, 43] studied the connection between \mathcal{NC} and generalization of overparameterized deep networks. Moreover, the works [43, 44, 45] demonstrated that the variability collapse of features is actually happening progressively from shallow to deep layers (with a linear decay rate), and [46] showed that test performance can be improved when enforcing variability collapse

¹We find that there is a certain threshold, that the transferability increases with the feature diversity below the threshold but decreases or becomes uncorrelated beyond it. Increasing the feature diversity will decrease the margin upon the threshold and hence the relationship with transferability becomes more involved with too large feature diversity.

on features of intermediate layers. The works [47, 48, 49] studied problems with imbalanced training data, showing that fixing the classifier as simplex ETFs improves test performance on imbalanced training data and long-tailed classification problems. For transferability, the work [7] implicitly showed that there is a tradeoff between variability collapse and transfer accuracy by experiments on a variety of loss functions.

- **Representation learning and model pre-training.** There are quite a few recent works studying the factors that affect transferability of pre-trained models, but the results are largely inconclusive. For example, the work [4] argues that models pre-trained on ImageNet with higher accuracy tend to perform better on other downstream tasks. However, such a conclusion has been challenged by more recent works [7, 50]. These results showed that the training loss and diversity of the features could be more important factors of transferability than the pre-trained accuracy. However, compared to our work, they only study few aspects (e.g., training loss) of deep network architectures that affect transferability, and they only focus on the diversity aspect on the source dataset. At the same time, the work [26] showed that models learned using contrastive type of loss functions could have better transferability, and [51] showed that their representations are more uniform over hyperspheres. The architecture and depth of CNNs were also shown to impact transfer performance [52]. Other work [53] exploited the importance of layers in overparameterized networks, suggesting the shallow and deep layers are more important in fine-tuning pre-trained models for downstream tasks.

Organizations. The rest of the paper is organized as follows. In Section 2, we provide a review of neural collapse, based upon which we introduce metrics for measuring the discrimination and diversity of learned representations for model transferability. In Section 3, based upon the metrics we run extensive experiments to demystify heuristics used in model pre-training, pointing to guiding principles for model fine-tuning. Finally, we conclude the work in Section 4. Extra experimental details are provided in the appendices.

2 Evaluating Representations of Pretrained Models via \mathcal{NC}

In this section, let us first give a brief overview of the \mathcal{NC} phenomenon, upon which we introduce the metrics for evaluating the quality of learned representations for transfer learning in Section 3.

Basics of deep neural networks. Let us first introduce some basic notations by considering a multi-class (e.g., K class) classification problem with finite training samples. Let $\{n_k\}_{k=1}^K$ be the number of training samples in each class. Let $\mathbf{x}_{k,i}$ denote the i th input data in the k th class ($1 \leq i \leq n_k, 1 \leq k \leq K$), and we use $\mathbf{y}_k \in \mathbb{R}^K$ to denote an one-hot training label with only the k th entry equal to unity. Thus, given any input data $\mathbf{x}_{k,i}$, we learn a deep network to fit the corresponding (one-hot) training label \mathbf{y}_k such that

$$\mathbf{y}_k \approx \psi_{\Theta}(\mathbf{x}_{k,i}) = \underset{\text{linear classifier } \mathbf{W}}{\mathbf{W}_L} \cdot \underset{\text{feature } \mathbf{h}_{k,i} = \phi_{\theta}(\mathbf{x}_{k,i})}{\sigma(\mathbf{W}_{L-1} \cdots \sigma(\mathbf{W}_1 \mathbf{x}_{k,i} + \mathbf{b}_1) + \mathbf{b}_{L-1}) + \mathbf{b}_L}, \quad (1)$$

where $\mathbf{W} = \mathbf{W}_L$ is the last-layer linear classifier and $\mathbf{h}_{k,i} = \mathbf{h}(\mathbf{x}_{k,i}) = \phi_{\theta}(\mathbf{x}_{k,i})$ denotes a deep hierarchical representation (or feature) of the input $\mathbf{x}_{k,i}$. Here, for a L -layer deep network $\psi_{\Theta}(\mathbf{x})$, each layer is composed of an affine transformation, followed by a nonlinear activation $\sigma(\cdot)$ and normalization functions (e.g., BatchNorm [54]). We use Θ to denote all the network parameters

of $\psi_{\Theta}(x)$ and θ to denote the network parameters of $\phi_{\theta}(x)$. Additionally, we use

$$\mathbf{H} = [\mathbf{H}_1 \ \mathbf{H}_2 \ \cdots \ \mathbf{H}_K] \in \mathbb{R}^{d \times N}, \quad \mathbf{H}_k = [\mathbf{h}_{k,1} \ \cdots \ \mathbf{h}_{k,n}] \in \mathbb{R}^{d \times n}, \quad 1 \leq k \leq K,$$

to denote all the features in the matrix form. Additionally, we write the class mean for each class as

$$\bar{\mathbf{H}} := [\bar{\mathbf{h}}_1 \ \cdots \ \bar{\mathbf{h}}_K] \in \mathbb{R}^{d \times K} \quad \text{and} \quad \bar{\mathbf{h}}_k := \frac{1}{n_k} \sum_{i=1}^{n_k} \mathbf{h}_{k,i}, \quad 1 \leq k \leq K.$$

Accordingly, we denote the global mean of \mathbf{H} as $\mathbf{h}_G = \frac{1}{K} \sum_{k=1}^K \bar{\mathbf{h}}_k$.

A review of the neural collapse. Over a balanced training dataset $\{\mathbf{x}_{k,i}, \mathbf{y}_k\}$ with $n = n_1 = n_2 = \cdots = n_K$, it has been widely observed that last-layer features \mathbf{H} and classifiers \mathbf{W} of a trained network exhibit simple but elegant mathematical structures [13, 44], that we highlight two key properties below.²

- **Intra-class variability collapse.** For each class, the last-layer features collapse to their means,

$$\mathbf{h}_{k,i} \rightarrow \bar{\mathbf{h}}_k, \quad \forall 1 \leq i \leq n, \ 1 \leq k \leq K. \quad (2)$$

- **Maximum between-class separation.** The class-means $\{\bar{\mathbf{h}}_k\}_{k=1}^K$ centered at their global mean \mathbf{h}_G are not only linearly separable, but are actually maximally distant and they form a Simplex Equiangular Tight Frame (ETF): for some $c > 0$, $\bar{\mathbf{H}} = [\bar{\mathbf{h}}_1 - \mathbf{h}_G \ \cdots \ \bar{\mathbf{h}}_K - \mathbf{h}_G]$ satisfies

$$\bar{\mathbf{H}}^\top \bar{\mathbf{H}} = \frac{cK}{K-1} \left(\mathbf{I}_K - \frac{1}{K} \mathbf{1}_K \mathbf{1}_K^\top \right). \quad (3)$$

Recent work shows that \mathcal{NC} persists across a range of canonical classification problems, on different loss functions (e.g., CE [13, 19], MSE [40, 17, 14], SupCon [19, 16]), different neural network architectures (e.g., VGG [55], ResNet [31], and DenseNet [32]), and a variety of standard datasets (e.g., MNIST [56], CIFAR [27], and ImageNet [57]). As we observe from above, although the maximum between-class separation suggests the learned features are discriminative in (3), the intra-class variability collapsing to a single dimension in (2) implies that the network is memorizing the labels rather than preserving the intrinsic structures of the data. As such, the loss of information of the input data could be detrimental for the transferability of the learned deep models. Nonetheless, the \mathcal{NC} phenomenon offers us good metrics for evaluating the transferability of pre-trained models that we discuss in the following.

Measuring feature quality via \mathcal{NC} metrics. Based upon above discussion, we can evaluate the transferability of pre-trained models by measuring the feature diversity and separation via metrics of evaluating \mathcal{NC} [13, 15], which defined as follows

$$\mathcal{NC}_1 := \frac{1}{K} \text{trace} \left(\Sigma_W \Sigma_B^\dagger \right). \quad (4)$$

²Additionally, self-duality convergence has also been observed in the sense that $\mathbf{w}_k = c' \bar{\mathbf{h}}_k$ for some $c' > 0$, but this is not the main focus of this work.

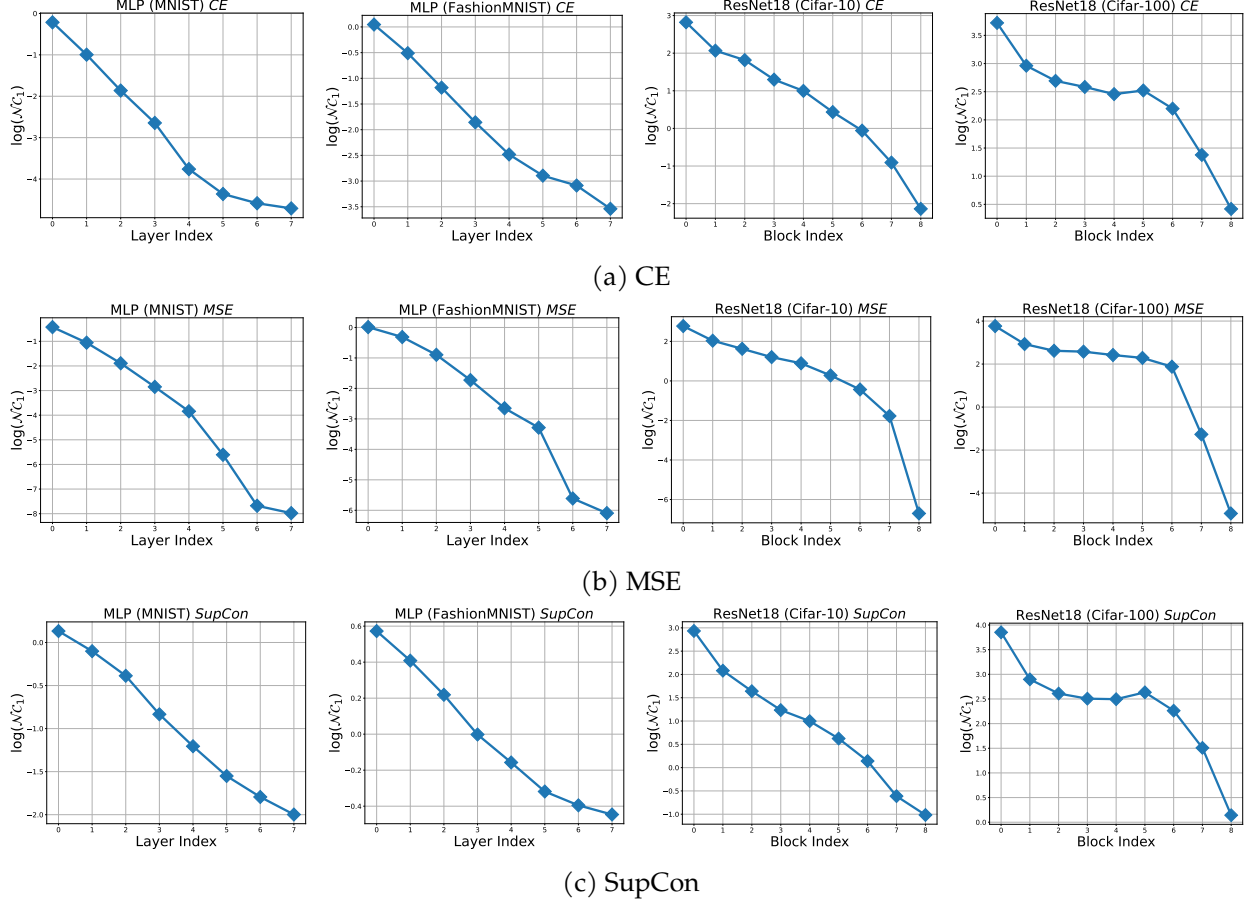


Figure 2: **Decay of the $\mathcal{N}C_1$ metric for well-trained MLP / ResNet18 models with different losses.** The MLP model is trained on MNIST [56] and FashionMNIST [58], respectively. The ResNet18 model is trained on Cifar-10 and Cifar-100. Prior to our work, similar results on the CE loss have been reported in [13, 43, 45], with linear convergence rate on MLP [45].

More specifically, it measures the magnitude of the within-class covariance $\Sigma_W \in \mathbb{R}^{d \times d}$ of the learned features compared to the inter-class covariance $\Sigma_B \in \mathbb{R}^{d \times d}$, where

$$\Sigma_W := \frac{1}{nK} \sum_{k=1}^K \sum_{i=1}^n (\mathbf{h}_{k,i} - \bar{\mathbf{h}}_k) (\mathbf{h}_{k,i} - \bar{\mathbf{h}}_k)^\top, \quad \Sigma_B := \frac{1}{K} \sum_{k=1}^K (\bar{\mathbf{h}}_k - \mathbf{h}_G) (\bar{\mathbf{h}}_k - \mathbf{h}_G)^\top.$$

Here, Σ_B^\dagger denotes the pseudo inverse of Σ_B , where Σ_B^\dagger serves as a normalization for Σ_W to capture the relativity between the two covariances. Intuitively, if the features of each class are more collapse to their corresponding class means, the smaller $\mathcal{N}C_1$ is; on the other hand, with the same Σ_W , if the features have more separated class means, $\mathcal{N}C_1$ would also be smaller. However, it should be noted that the metric involves pseudo inverse of Σ_B , computation of such a metric in (4) could be very expensive when the feature dimension is large, which could be true for huge models. To deal with issue, we also introduced alternative metrics such as class-distance normalized variance (CDNV) [42] and numerical rank [17], that we refer readers to Appendix A for more detail.

Progressive neural collapse across layers. So far, various works [13, 14] have shown that \mathcal{NC}_1 metric converges to zero when evaluated on the last-layer feature

$$\mathbf{h} = \sigma(\mathbf{W}_{L-1} \cdots \sigma(\mathbf{W}_1 \mathbf{x} + \mathbf{b}_1) + \mathbf{b}_{L-1}).$$

More surprisingly, when the \mathcal{NC}_1 evaluated on the feature $\mathbf{h}^\ell = \sigma(\mathbf{W}_{\ell-1} \cdots \sigma(\mathbf{W}_1 \mathbf{x} + \mathbf{b}_1) + \mathbf{b}_{\ell-1})$ across all intermediate layers ($1 \leq \ell \leq L-1$), it can be further shown that it progressively decays from shallow to deep layers of a well-trained overparamterized deep neural network [13, 43, 45], as we illustrate in Figure 2. Similar to \mathcal{NC} , the layer-wise progressive collapse is universal, where it is also prevalent across the choice of training losses, network architectures, and dataset. Moreover, the recent work [59] showed that the decay rate could be linear for simple networks such as MLPs, VGGs, and ResNet. The progressive decay of feature diversity implies that the deep network is discarding information of the input data from shallow to deep layers. In the following section, we will show that this observation would be very useful for explaining heuristic methods in pre-training and designing more efficient fine-tuning methods in a principled manner.

3 Methods & Experiments

In the following, we will utilize the above metric (4) to evaluate the quality of learned representations for transfer learning, providing new insights for pre-training and fine-tuning. More specifically, in Section 3.1 we investigate the relationship between model transferability and their \mathcal{NC} metrics in pre-training, explaining common heuristics in pre-training such as the usage of projection head and the choices of training losses. In Section 3.2, we turn our attention to downstream tasks, where we find that the \mathcal{NC} metrics and the associated transfer accuracy are negatively correlated: smaller \mathcal{NC}_1 on downstream data results in better transfer accuracy. In Section 3.3, based on the above findings via \mathcal{NC} , we propose a simple and efficient fine-tuning method on downstream dataset, even outperforming fully fine-tuning. The details of all the experimental setup are postponed to Appendix B.

3.1 Study of \mathcal{NC} & Transfer Accuracy on Model Pre-training

We begin our investigation by studying the relationship between \mathcal{NC} metrics on *pre-training dataset* and transfer accuracy. Within a certain range,³ we show that the two are positively correlated – larger \mathcal{NC} metrics leads to better transfer accuracy, which echoes similar discoveries in recent work [26, 7]. The intuition is that if the learned representations are less collapsed on the pre-trained data, they better preserve the intrinsic structures of the input data. Moreover, compared to [26, 7], our work not only studies the effect of different training losses on feature diversity, but also (i) provides insights for several heuristics in model pre-training (e.g., projection head, data augmentation), and (ii) reveals the limitations of merely using feature diversity as the metric for evaluating representation quality for transfer learning.

Choices of training losses and architectures impact feature diversity and hence transferability. First, we show that the choice of training losses and design of architecture substantially affects the collapse of the features on the penultimate layer, and hence the transfer accuracy.⁴ To show this, we

³As random features do not collapse but not generalize well, the positive correlation above only holds to a certain extent. The reason is that random features are not discriminative. We conjecture that there could be a trade-off between feature diversity and discrimination.

⁴For the choices of loss, the works [26, 7] have similar observations, where different choices of training losses for pre-training lead to different transfer performance.

Training	MSE (w/o proj.)	Cross-entropy (w/o proj.)	SupCon (w/ linear proj.)	SupCon (w/ mlp proj.)
\mathcal{NC}_1 (Cifar-100)	0.001	0.771	0.792	2.991
Transfer Acc.	53.96	71.2	69.89	79.51

Table 1: **Transfer learning results & model \mathcal{NC}_1 comparison among different training settings.** ResNet18 models are pre-trained on the Cifar-100 dataset and transfered on Cifar-10. We use proj. to denote projection head. w/o proj. means without projection head, w/linear proj. means adding one linear layer projection layer, and w/ mlp proj. means adding a two-layer MLP projection.

pre-train ResNet18 models on the Cifar-100 dataset with three different choices of loss functions: CE, MSE [22], and SupCon [9]). Once the model is trained, we evaluate the test accuracy on the Cifar-10 dataset, by only learning a linear classifier upon the frozen pre-trained models. In Table 1, we summarize the results of \mathcal{NC}_1 of all pre-trained models and the corresponding transfer accuracy for different training scenarios. For the SupCon loss [9], in particular, we also follow the original setup by using a nonlinear multi-layer perceptron (MLP) module as a projection head after the ResNet18 encoder. More specifically, once the model has been pre-trained, the projection head will be abandoned and only the encoder network will be utilized as the pre-trained model for downstream tasks. The results are reported in the last two columns of Table 1, with adding one-layer linear projection and multiple-layer MLP projection, respectively. As we observe from Table 1,

- Different training losses affect the feature diversity, and hence transfer accuracy, where losses with larger feature diversity (larger \mathcal{NC}_1) lead to better transfer accuracy. For instance, the model pre-trained with the MSE loss is severely collapsed on the source dataset (smallest \mathcal{NC}_1 , showing the worst transfer accuracy).
- The MLP projection head plays an important role for better transferability. The model pre-trained using the SupCon with a multi-layer MLP projection head has the least collapsed features compared to the other models, and it demonstrates superior transfer performance.⁵ When we replace the MLP with a linear projection layer, both the \mathcal{NC}_1 and transfer accuracy SupCon decrease, showing on-par performance with the model trained using the CE loss.

Based upon the above observation, in the following we further demystify the role of projection head for transfer learning through the phenomenon of progressive \mathcal{NC} across layers.

Projection layers in pre-training increase feature diversity for better transferability. The usage of projection head for model pre-training is first introduced and then popularized for self-supervised learning [8, 23], but the reason why it works is not very well understood. Here, we demystify the underlying mechanism of projection head based upon progressive variability collapse. As shown in recent works [44, 43, 59] and our experiments in Figure 2, the within-class variability collapse actually happens progressively from shallow to deep layers: the closer to the final layer, the severer the variability collapse is (i.e., the smaller the \mathcal{NC}_1 of the corresponding layer). Therefore, for model pre-training,

The usage of additional MLP projection layers prevents variability collapse of the features of the encoder network for better preserving the information of input data, resulting in better transfer performance.

⁵This observation is consistent with [26].

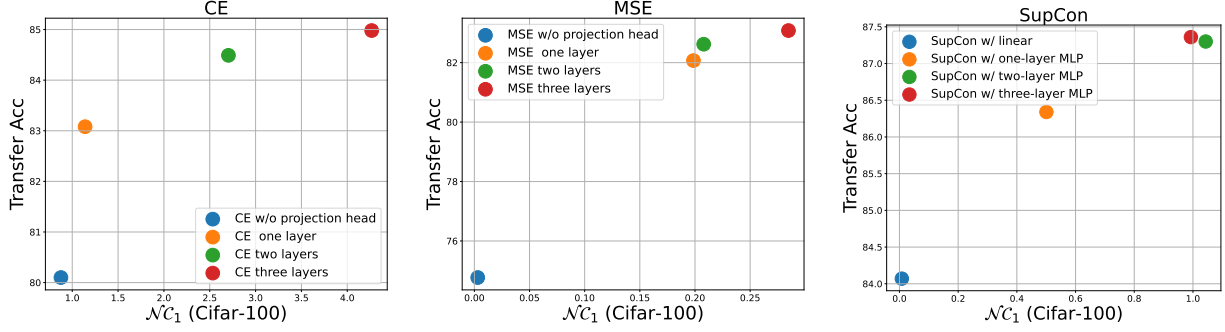


Figure 3: **Trend of \mathcal{NC}_1 during training and transfer learning accuracy of the pretrained models.** ResNet50 models are pretrained using Cifar-100 dataset with CE loss (Left), MSE loss (Middle) and SupCon loss (Right). Models are pretrained with different numbers of layers for projection heads and transferred on the Cifar-10 dataset.

This can be demonstrated by our experiments in Figure 3, where we pre-train ResNet-50 models (we use it for better performance) on the Cifar-100 dataset and report the \mathcal{NC} and transfer accuracy for a different number of layers of projection heads (from one to three layers). We show that the usage of projection heads substantially increases the diversity of the representations and the transfer accuracy – more layers of MLP projection lead to larger \mathcal{NC}_1 , and hence better transfer accuracy. Additionally, the performance gain quickly saturates upon three layers of MLP. The phenomenon is quite universal across different training losses (i.e., CE, MSE, and SupCon), which also suggests that the effectiveness of projection heads for model pre-training is not limited to contrastive losses.

Usage of the pre-trained \mathcal{NC} metric for predicting transfer accuracy has limitations. So far, we have *seemingly* demonstrated an universal positive correlation between the \mathcal{NC}_1 and transferability. However, does the increase for the \mathcal{NC}_1 of learned features always lead to improved model transferability? To more comprehensively characterize the relationship between \mathcal{NC}_1 and transferability, we pre-train ResNet50 models on the Cifar-100 dataset using different levels of data augmentations and adversarial training [60, 24, 25] strength,⁶ and then test the transfer accuracy on the Cifar-10 dataset. The results are shown in Figure 4. Our observation is that the positive relationship between the \mathcal{NC}_1 on the source dataset and the transfer accuracy only holds up to a certain threshold.⁷ If the \mathcal{NC}_1 metric is larger than a certain threshold, the transfer accuracy decreases as the \mathcal{NC}_1 increases.

We conjecture the reason behind the limitation is that the magnitude of \mathcal{NC}_1 is affected by two factors of the learned features: (i) within class feature diversity and (ii) between class discrimination, and the loss of the latter would also increase

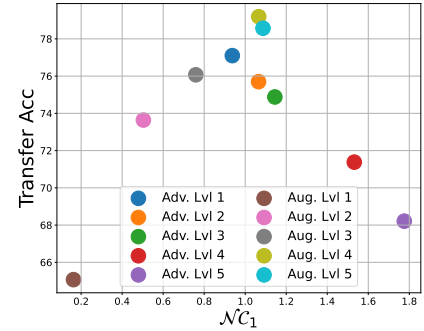


Figure 4: **\mathcal{NC}_1 vs. Transfer learning accuracy.** Models are pretrained using the Cifar-100 dataset with different data augmentation levels and adversarial training strength, transfer accuracy is evaluated on the Cifar-10 dataset.

⁶We use 5 levels of data augmentations, each level represents adding one additional type of augmentation, e.g., Level 1 means Normalization, level 2 means Normalization + RandomCrop, etc. For adversarial training strength, we follow the framework in [60] and consider 5 different attack sizes. Please refer to Appendix B for more details.

⁷The work [7] studied the transferability based upon a notion called class separation, which is similar to \mathcal{NC}_1 . However, the work only studied the relationship within a limited range of class separation, which excludes the case of zero class separation.

\mathcal{NC}_1 but decrease the transferability. An extreme example would be an untrained deep model with randomly initialized weights, which obviously possesses large \mathcal{NC}_1 with large feature diversity and poor feature discrimination. Obviously, random features have poor transferability. Therefore, to better predict the model transferability, we need more precise metrics of both within-class feature diversity and between-class discrimination, which could have a tradeoff. We leave the investigation as future work.

3.2 Study of \mathcal{NC} & Transfer Accuracy on Downstream Tasks

Second, given the pre-trained models, on *downstream data* we experimentally investigate the relationship between \mathcal{NC}_1 metric of their representations and transfer accuracy. Transferring pre-trained large models to smaller downstream tasks has become the dominant approach in both vision [12] and language [2] domains. Moreover, because of the huge size and the limited access nature of the source datasets,⁸ it is often intractable to get the statistics of the \mathcal{NC}_1 metric on the source datasets. They both motivate us to study the \mathcal{NC}_1 metric on the downstream data.

Here, to limit the factors affecting our study, for each downstream task we *freeze* the whole pre-trained model without fine-tuning, upon which we only train a linear classifier using the downstream data. In contrast to Section 3.1, on downstream data, we find that the transfer accuracy is negatively correlated with the \mathcal{NC}_1 metric. Moreover, we show that this phenomenon is also quite universal: it not only happens among pre-trained models with different pre-training strategies but also across different layers of the same pre-trained models.

Pre-trained models with more collapsed last-layer features result in better transferability. To validate our statement, we pre-train different ResNet50 models on the Cifar-100 dataset by using different levels of data augmentations and different levels of adversarial training strength. Once a model is pre-trained, we test its transfer accuracy on 4 downstream datasets: Cifar-10 [27], FGVS-Aircraft [28], DTD [29] and Oxford-IIIT-Pet [30] datasets. In Figure 5, we observe that the \mathcal{NC}_1 on Cifar-10 dataset has a negative (almost linear) correlation with the transfer accuracy on these downstream tasks. The smaller \mathcal{NC}_1 on the Cifar-10 dataset, the higher the transfer accuracy.⁹ As such, the \mathcal{NC}_1 metric on Cifar-10 evaluated on pre-trained models can serve as a good performance indicator for the transfer accuracy on downstream tasks. To further strengthen our argument, we conduct experiments on the same set of downstream tasks using publicly available pre-trained models on ImageNet-1k [57], such as ResNet [31], DenseNet [32] and MobileNetV2 [33]. We observe the same negative correlation between \mathcal{NC}_1 and transfer accuracy in Figure 6. This implies that such a relationship not only exists across different training scenarios of the same network but also exists more universally across different network architectures.

The opposite relationships on pre-trained data compared to downstream data between the \mathcal{NC}_1 metric and transfer accuracy may seem contradictory at first glance. Intuitively, for pre-training on source data, as we explained in Section 3.1, we desire more diverse features (large \mathcal{NC}_1) so that the learned features can capture the structure of the input data. In contrast, on downstream data, for classification, we desire a large margin, and small \mathcal{NC}_1 often implies that the margin is large. Moreover, we also observe that pre-trained models with larger \mathcal{NC}_1 on source data could translate to smaller \mathcal{NC}_1 on downstream data and hence better transfer accuracy.

⁸e.g., JFT dataset [61], which is used in the pretraining of Vision Transformer, is not publicly available.

⁹When evaluating the relationship between \mathcal{NC}_1 and transfer accuracy measured on the same downstream dataset, the correlation is not as strong as we find on Cifar-10 dataset, we leave the results and discussion in Appendix C.

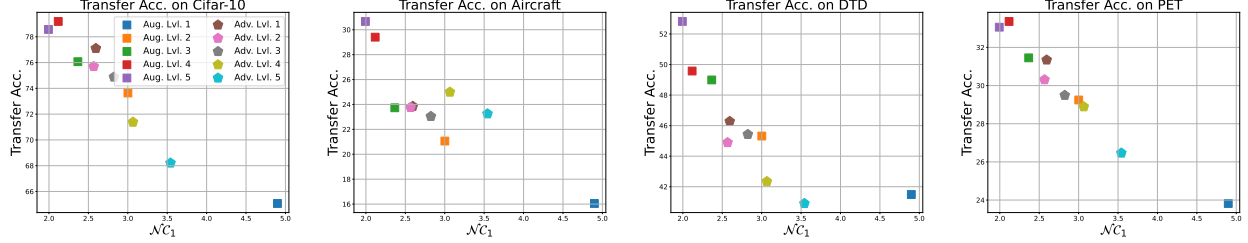


Figure 5: **Transfer accuracy on different downstream tasks and $\mathcal{N}C_1$.** We pre-train ResNet50 models on Cifar-100 using different levels of data augmentation or adversarial training. $\mathcal{N}C_1$ is measured on the downstream Cifar-10 dataset.

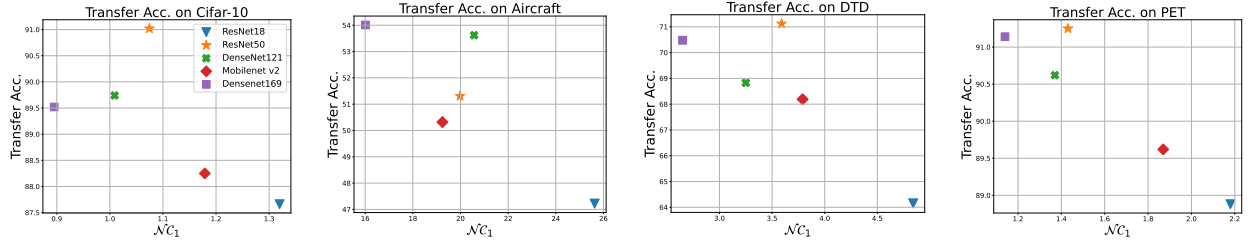


Figure 6: **Transfer accuracy on different downstream tasks and $\mathcal{N}C_1$.** We evaluate transfer accuracy and $\mathcal{N}C_1$ on multiple downstream datasets using various ImageNet-1k pre-trained models. $\mathcal{N}C_1$ is measured on the corresponding downstream dataset.

Layers with more collapsed output features result in better transferability. More intriguingly, the phenomenon we observed above not only happens among different pre-trained models, but also happens across (the outputs of) different layers on exactly the same pre-trained model. More precisely, as shown in Figure 7, we use the output of each individual layer of the same pre-trained model as a “feature extractor”, and we test the transfer accuracy of the given layer by training a linear classifier on top of it. Surprisingly, if the outputs of the layer are more collapsed, using the corresponding features leads to better transfer accuracy, which happens regardless of the layer’s depth.

To corroborate our claim, we use an ImageNet-1k [57] pre-trained ResNet34 [31] model and we evaluate the $\mathcal{N}C_1$ metric on each residual block’s output feature upon the downstream data. Additionally, we conducted similar experiments on ViT-B (vision transformer base model) [12] by using a pre-trained checkpoint released online¹⁰. As we observe in Figure 8, layers with smaller $\mathcal{N}C_1$ of the output features result in better transfer accuracy. Moreover, we can observe a near linear relationship between $\mathcal{N}C_1$ and transfer accuracy. Therefore, the transfer accuracy is more related to the variability collapse upon the layer rather than the depth of the layer, and such a phenomenon holds universally from ResNet to ViT models.

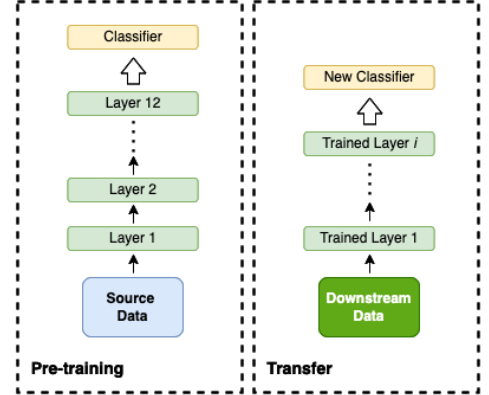


Figure 7: **An illustration of layer-wise transfer learning.** We use the outputs from each layer of the pre-trained models to do transfer learning.

¹⁰The ViT-B model checkpoint we used could be found [here](#).

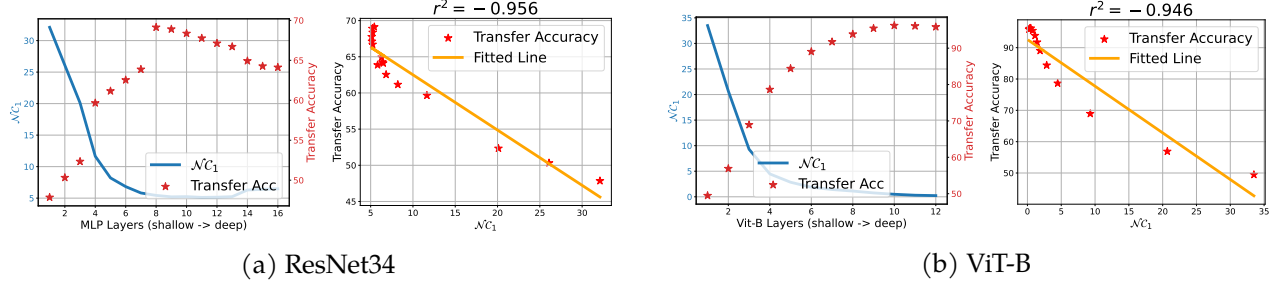


Figure 8: $\mathcal{N}C_1$ and transfer learning accuracy of different layers from a pre-trained model (Left) and nearly linear relationship between transfer learning accuracy and $\mathcal{N}C_1$ (Right). We use (a) an ImageNet-1k dataset pre-trained ResNet34 model and (b) a released pre-trained ViT-B model. We use the Cifar-10 dataset for transfer learning and measuring the corresponding $\mathcal{N}C_1$.

3.3 A Simple & Efficient Fine-tuning Strategy for Improving Transferability

Finally, we demonstrate that the phenomenon we discovered in Section 3.2 can be very useful for designing simple yet efficient fine-tuning strategies without sacrificing the performance (compared to fully fine-tune). For vision tasks, transfer learning typically adopts two strategies: (i) **fixed feature training** [9, 7, 25], use pre-trained model up to the penultimate layer as a feature extractor and only train a new linear classifier on top of the features for a downstream task; (ii) **full model fine-tuning** [12, 4, 24], use the pre-trained model as initialization and fine-tune the whole model to fit a downstream task. However, the full fine-tuning could be very expensive especially for large models, while fixed feature training, without adapting the model to the downstream data, often results in worse performance. To deal with the disadvantages of both methods, for vision problems one promising but seldom explored approach is to only fine-tune selective layers [62, 63]. Based upon the correlation between penultimate layer collapse and the transfer learning performances in Section 3.2, our conjecture is that

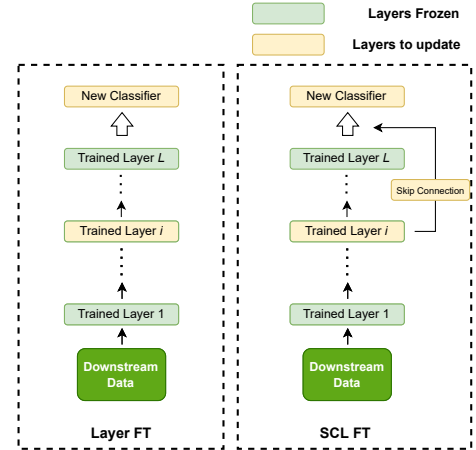


Figure 9: Illustrations of Layer FL (left) and SCL FT (right).

The topmost transfer accuracy can be achieved by selectively fine-tuning the layers such that the features of penultimate layer are the most collapsed on the downstream training data.

To increase the level of collapse of the penultimate layer, we propose two simple fine-tuning strategies that we describe in the following. All experimental results for both methods are summarized in Table 2, where the two methods can achieve on-par or even better transfer accuracy compared to fully fine-tuning.

- **Layer fine-tuning (FT).** As shown in Table 2, we demonstrate that the collapse of penultimate layer features can be achieved simply by fine-tuning *only* one of the intermediate layers while keeping the rest of the network frozen (see Figure 9 (left)). On top of that, our experiments show that fine-tuning one of the top layers near the penultimate layer often yields the best re-

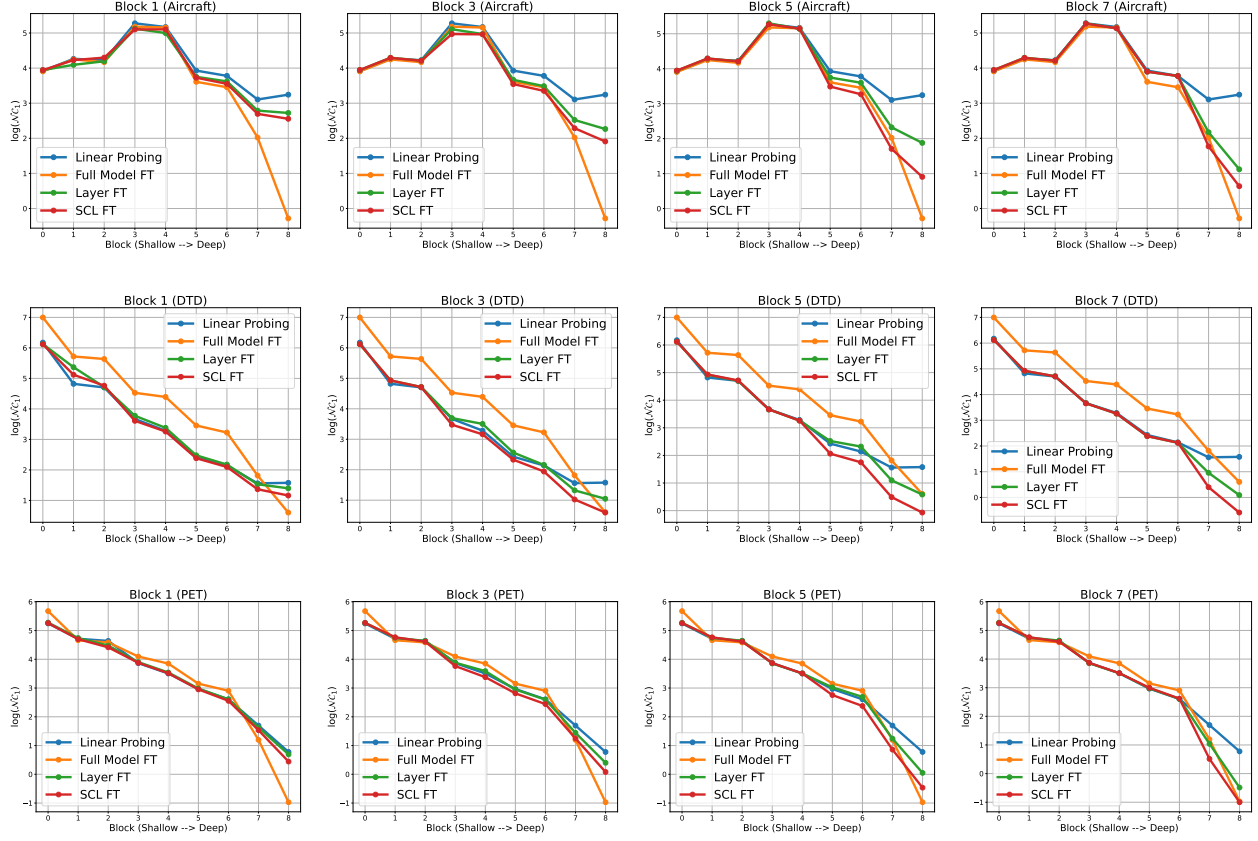


Figure 10: **Layer-wise $\mathcal{N}C_1$ for different fine-tuning methods.** Based on the ResNet18 backbone, We plot and compare the layer-wise $\mathcal{N}C_1$ across layers for pre-trained models for linear probing (i.e., pre-training), Layer FT, and SCL FT. For Layer FT, and SCL FT, we plot 4 figures (from left to right) for only fine-tuning Block 1, Block 3, Block 5, and Block 7. Transfer accuracy and $\mathcal{N}C_1$ are measured on the FGVS-Aircraft dataset (Top), DTD dataset (Middle), and Oxford-IIIT-Pet dataset (Bottom), respectively.

sult universally.¹¹ Although this is still empirical, hypothetically we believe this is because, at the position of the top layers in a network, the information from the inputs has already been extracted and distilled, and hence fine-tuning such a layer is the most effective. As we observe from Table 2, on both ResNet and ViT network architectures, this simple Layer FT approach already leads to substantial performance gain compared with vanilla linear probing (i.e., fixed feature training) universally on a variety of downstream datasets including Cifar [27], FGVS-Aircraft [28], DTD [29] and Oxford-IIIT-Pet [30] datasets.

- **Skip connection layer (SCL) fine-tuning (FT).** Based upon the Layer FT, as shown in Figure 9 (right), we can further improve its performance by adding a skip connection from the fine-tuned layer to the penultimate layer, and using the combined features of those two layers (i.e., adding the output features of the two layers together¹²) as the new feature for the final linear classifier.

¹¹As shown in Tables 3 to 5, we find fine-tuning Block 7 for ResNet18 (8 blocks in total), Block 14 for ResNet50 (16 blocks in total) and Layer 11 for ViT model (12 layers in total) always yields the best or near-optimal results.

¹²For ResNet, if the feature dimensions are different, we can do zero-padding of the lower dimensional feature to compensate for the dimensional difference. We refer to Appendix B for more details.

Backbone	ResNet18					ResNet50					ViT-B		
Dataset	Cifar-10	Cifar-100	Aircraft	DTD	PET	Cifar-10	Cifar-100	Aircraft	DTD	PET	Aircraft	DTD	PET
Transfer Acc.													
Linear Probe	81.64	59.75	38.94	60.16	86.26	85.33	65.47	43.23	68.46	89.26	43.65	73.88	92.23
Layer FT	93.08	75.04	68.65	68.56	88.01	94.04	77.82	72.67	71.81	90.13	65.83	77.13	93.02
SCL FT	93.65	75.69	70.24	71.22	89.78	94.94	78.40	74.26	74.89	91.71	65.80	77.34	93.19
Full Model FT	92.11	78.65	78.25	41.38	74.24	85.51	78.88	80.77	38.83	73.24	64.66	76.49	93.02
Penultimate \mathcal{NC}_1													
Linear Probe	1.82	22.72	22.50	4.51	2.32	1.84	18.36	20.36	3.52	1.45	17.91	1.99	0.66
Layer FT	0.22	1.60	2.47	1.10	1.49	0.28	7.72	1.27	0.78	0.32	0.13	1.62	0.44
SCL FT	0.16	1.43	1.43	0.56	0.63	0.22	7.24	0.37	0.51	0.16	0.10	1.33	0.40
Full Model FT	0.08	0.39	0.75	1.83	0.38	0.17	0.15	0.61	1.85	0.28	0.11	1.11	0.21

Table 2: **Transfer learning results for Linear probing, layer fine-tuning, SCL fine-tuning and full model fine-tuning on various downstream datasets.** We use released ResNet models pre-trained on ImageNet-1k [57] and ViT-B model pre-trained on JFT [61] and ImageNet-21k [64] datasets.

Such a method enables the network to more effectively fine-tune the selected layer by explicitly passing the information of the data from the intermediate layer to the classifier, without suffering information loss through the cascade of intermediate layers. Additionally, instead of throwing away layers above the fine-tuned layers, the method also enjoys the benefits of depth of the deep models, which intuitively makes the features more linearly separable across layers. From Table 2, for both ResNet and ViT network architectures, we observe that SCL FT nearly always outperforms Layer FT and achieves comparable or even better results compared with full model FT on a variety of datasets.

Dramatically improved memory efficiency and less overfitting compared to Full FT. Full model FT means re-training all the 23M parameters for ResNet50, or 88M parameters for ViT-B32. Our methods are much cheaper, as shown in Tables 3 to 5, with *only* around 8% parameters of an entire model fine-tuned, layer FT and SCL FT can achieve on-par or superior performances compared with full model FT. Furthermore, our proposed methods are less likely to overfit compared with the full FT. In the limited data regime, fine-tuning the whole model on the downstream training dataset could lead to severe overfit and result in inferior generalization performance. Our methods, on the other hand, are more robust to data scarcity since only a small percentage of parameters are being changed. To verify the robustness of our methods, we fine-tune pre-trained models on different subsets of training samples of Cifar-10 and report the results in Figure 11. We can observe that the full model FT indeed suffers from data scarcity and performs worse than linear probing when data is insufficient while layer FT and SCL FT are more robust and constantly outperform full model FT until the data quantity becomes very abundant.

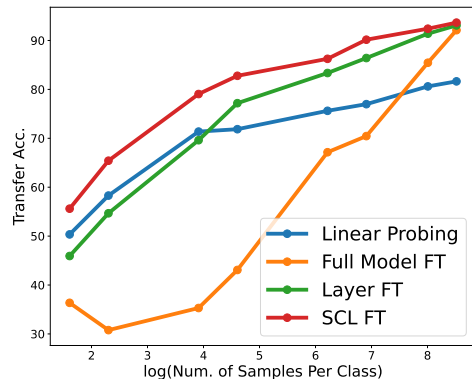


Figure 11: **Trend of transfer performances for different fine-tuning methods with the change of training dataset size.** ImageNet-1k pre-trained ResNet18 models are fine-tuned on subsets of Cifar-10 training dataset.

4 Discussion & Conclusion

In this work, we have provided a comprehensive study between \mathcal{NC} and transferability by showing the twofold relationship: (i) models that are less collapsed on the *source* data have better transferability to a certain threshold; (ii) more collapsed features on the *downstream* data leads to better transfer performance and such relationship holds both across and within models. Inspired by the negative relationship between downstream \mathcal{NC} and transfer performance, we propose a simple yet effective model fine-tuning method without adding additional parameters to the model or changing the training process. We further empirically verify our proposed method can achieve on-par or even superior performances compared with full model fine-tuning across various tasks and setups. Our findings also open up potential research directions which we summarize in the following.

Neuron collapse beyond optimization. Previous work [43] points out that \mathcal{NC} is mainly an optimization phenomenon that does not necessarily relate to generalization (or transferability). Our work, on one hand, corroborates with the finding that pretraining \mathcal{NC} does not always suggest better transferability, but also shows a positive correlation between pretraining \mathcal{NC} and transferability to a certain extent. On the other hand, our work also shows that downstream \mathcal{NC} on a dataset where \mathcal{NC} is well-defined correlates with the transfer performances across different datasets and thus could be a general indicator for the transferability. This suggests that \mathcal{NC} may not be merely an optimization phenomenon. An important future direction we will pursue is to theoretically understand the connection between transferability and \mathcal{NC} .

Boost model transferability by insights from \mathcal{NC} . Our findings can be used to improve model transferability through the following two perspectives. First, the positive correlation between pretraining \mathcal{NC} and transferability suggests that increasing \mathcal{NC}_1 of features to a certain extent can improve transferability. This can be achieved by popular techniques such as multi-layer projection heads and data augmentation. We believe other principled approaches could also be developed by explicitly working on the geometry of the representations. Second, by demonstrating the close correlation between downstream \mathcal{NC} and associated transfer accuracy, we can develop simple yet effective strategies for efficient transfer learning. However, our simple approach is by no means the optimal method to exploit such a relationship of \mathcal{NC} . We believe there are more powerful approaches that could utilize this phenomenon better and thus achieves better transferability. We leave this as future work.

Transfer learning beyond \mathcal{NC} . Our results suggest that \mathcal{NC} on the source datasets correlates with transferability up to some threshold. However, locating the threshold and explaining the change in transferability above the threshold are challenging under the \mathcal{NC} framework. Furthermore, using \mathcal{NC} alone to study transfer learning could be off-the-shelf in some circumstances. For example, recent work [51] showed that representations learned from unsupervised contrastive approaches are uniform over hyperspheres and [65] illustrated that representations learned using the maximal coding rate reduction (MCR²) principle forming subspaces instead of collapsing to single points. Therefore, further disclosing the mysteries shrouded around transfer learning would require new frameworks and new tools, which we leave for future investigation.

Acknowledgement

XL and QQ acknowledge generous support from U-M START & PODS grants, a gift fund from KLA, NSF CAREER CCF 2143904, NSF CCF 2212066, NSF CCF 2212326, and ONR N00014-22-1-2529. JZ and ZZ acknowledge support from NSF grants CCF-2240708 and CCF-2241298. SL acknowledges support from NSF NRT-HDR Award 1922658 and Alzheimer’s Association grant AARG-NTF-21-848627, and CFG acknowledges support from NSF OAC-2103936. We thank Dr. Chong You (Google Research), Dr. Hongyuan Mei (TTIC) for fruitful discussions at various stages of the work.

References

- [1] F. Zhuang, Z. Qi, K. Duan, D. Xi, Y. Zhu, H. Zhu, H. Xiong, and Q. He, “A comprehensive survey on transfer learning,” *Proceedings of the IEEE*, vol. 109, no. 1, pp. 43–76, 2020.
- [2] J. Devlin, M.-W. Chang, K. Lee, and K. Toutanova, “Bert: Pre-training of deep bidirectional transformers for language understanding,” *ArXiv*, vol. abs/1810.04805, 2019.
- [3] V. Cheplygina, M. de Bruijne, and J. P. Pluim, “Not-so-supervised: A survey of semi-supervised, multi-instance, and transfer learning in medical image analysis,” pp. 280–296, 2019.
- [4] S. Kornblith, J. Shlens, and Q. V. Le, “Do better imagenet models transfer better?,” in *Proceedings of the IEEE/CVF conference on computer vision and pattern recognition*, pp. 2661–2671, 2019.
- [5] C. Szegedy, V. Vanhoucke, S. Ioffe, J. Shlens, and Z. Wojna, “Rethinking the inception architecture for computer vision,” *2016 IEEE Conference on Computer Vision and Pattern Recognition (CVPR)*, pp. 2818–2826, 2016.
- [6] N. Srivastava, G. Hinton, A. Krizhevsky, I. Sutskever, and R. Salakhutdinov, “Dropout: A simple way to prevent neural networks from overfitting,” *Journal of Machine Learning Research*, vol. 15, no. 56, pp. 1929–1958, 2014.
- [7] S. Kornblith, T. Chen, H. Lee, and M. Norouzi, “Why do better loss functions lead to less transferable features?,” in *NeurIPS*, 2021.
- [8] T. Chen, S. Kornblith, M. Norouzi, and G. E. Hinton, “A simple framework for contrastive learning of visual representations,” *ArXiv*, vol. abs/2002.05709, 2020.
- [9] P. Khosla, P. Teterwak, C. Wang, A. Sarna, Y. Tian, P. Isola, A. Maschinot, C. Liu, and D. Krishnan, “Supervised contrastive learning,” *arXiv preprint arXiv:2004.11362*, 2020.
- [10] T. B. Brown, B. Mann, N. Ryder, M. Subbiah, J. Kaplan, P. Dhariwal, A. Neelakantan, P. Shyam, G. Sastry, A. Askell, S. Agarwal, A. Herbert-Voss, G. Krueger, T. J. Henighan, R. Child, A. Ramesh, D. M. Ziegler, J. Wu, C. Winter, C. Hesse, M. Chen, E. Sigler, M. Litwin, S. Gray, B. Chess, J. Clark, C. Berner, S. McCandlish, A. Radford, I. Sutskever, and D. Amodei, “Language models are few-shot learners,” *ArXiv*, vol. abs/2005.14165, 2020.
- [11] A. Vaswani, N. M. Shazeer, N. Parmar, J. Uszkoreit, L. Jones, A. N. Gomez, L. Kaiser, and I. Polosukhin, “Attention is all you need,” in *NIPS*, 2017.
- [12] A. Dosovitskiy, L. Beyer, A. Kolesnikov, D. Weissenborn, X. Zhai, T. Unterthiner, M. Dehghani, M. Minderer, G. Heigold, S. Gelly, J. Uszkoreit, and N. Houlsby, “An image is worth 16x16 words: Transformers for image recognition at scale,” *ArXiv*, vol. abs/2010.11929, 2021.
- [13] V. Pappayan, X. Han, and D. L. Donoho, “Prevalence of neural collapse during the terminal phase of deep learning training,” *Proceedings of the National Academy of Sciences*, vol. 117, no. 40, pp. 24652–24663, 2020.
- [14] X. Han, V. Pappayan, and D. L. Donoho, “Neural collapse under MSE loss: Proximity to and dynamics on the central path,” in *International Conference on Learning Representations*, 2022.

- [15] Z. Zhu, T. Ding, J. Zhou, X. Li, C. You, J. Sulam, and Q. Qu, "A geometric analysis of neural collapse with unconstrained features," *Advances in Neural Information Processing Systems*, vol. 34, 2021.
- [16] F. Graf, C. Hofer, M. Niethammer, and R. Kwitt, "Dissecting supervised contrastive learning," in *International Conference on Machine Learning*, pp. 3821–3830, PMLR, 2021.
- [17] J. Zhou, X. Li, T. Ding, C. You, Q. Qu, and Z. Zhu, "On the optimization landscape of neural collapse under mse loss: Global optimality with unconstrained features," in *International Conference on Machine Learning*, 2022.
- [18] J. Zhou, C. You, X. Li, K. Liu, S. Liu, Q. Qu, and Z. Zhu, "Are all losses created equal: A neural collapse perspective," *arXiv preprint arXiv:2210.02192*, 2022.
- [19] C. Fang, H. He, Q. Long, and W. J. Su, "Exploring deep neural networks via layer-peeled model: Minority collapse in imbalanced training," *Proceedings of the National Academy of Sciences*, vol. 118, no. 43, 2021.
- [20] T. Tirer and J. Bruna, "Extended unconstrained features model for exploring deep neural collapse," *arXiv preprint arXiv:2202.08087*, 2022.
- [21] C. Yaras, P. Wang, Z. Zhu, L. Balzano, and Q. Qu, "Neural collapse with normalized features: A geometric analysis over the riemannian manifold," *arXiv preprint arXiv:2209.09211*, 2022.
- [22] L. Hui and M. Belkin, "Evaluation of neural architectures trained with square loss vs cross-entropy in classification tasks," *arXiv preprint arXiv:2006.07322*, 2020.
- [23] X. Chen and K. He, "Exploring simple siamese representation learning," *2021 IEEE/CVF Conference on Computer Vision and Pattern Recognition (CVPR)*, pp. 15745–15753, 2021.
- [24] H. Salman, A. Ilyas, L. Engstrom, A. Kapoor, and A. Madry, "Do adversarially robust imagenet models transfer better?," in *ArXiv preprint arXiv:2007.08489*, 2020.
- [25] Z. Deng, L. Zhang, K. Vodrahalli, K. Kawaguchi, and J. Zou, "Adversarial training helps transfer learning via better representations," in *Advances in Neural Information Processing Systems* (A. Beygelzimer, Y. Dauphin, P. Liang, and J. W. Vaughan, eds.), 2021.
- [26] A. Islam, C.-F. R. Chen, R. Panda, L. Karlinsky, R. Radke, and R. Feris, "A broad study on the transferability of visual representations with contrastive learning," in *Proceedings of the IEEE/CVF International Conference on Computer Vision*, pp. 8845–8855, 2021.
- [27] A. Krizhevsky, G. Hinton, *et al.*, "Learning multiple layers of features from tiny images," 2009.
- [28] S. Maji, J. Kannala, E. Rahtu, M. Blaschko, and A. Vedaldi, "Fine-grained visual classification of aircraft," *tech. rep.*, 2013.
- [29] M. Cimpoi, S. Maji, I. Kokkinos, S. Mohamed, , and A. Vedaldi, "Describing textures in the wild," in *Proceedings of the IEEE Conf. on Computer Vision and Pattern Recognition (CVPR)*, 2014.
- [30] O. M. Parkhi, A. Vedaldi, A. Zisserman, and C. V. Jawahar, "Cats and dogs," in *IEEE Conference on Computer Vision and Pattern Recognition*, 2012.
- [31] K. He, X. Zhang, S. Ren, and J. Sun, "Deep residual learning for image recognition," in *Proceedings of the IEEE conference on computer vision and pattern recognition*, pp. 770–778, 2016.
- [32] G. Huang, Z. Liu, L. Van Der Maaten, and K. Q. Weinberger, "Densely connected convolutional networks," in *Proceedings of the IEEE conference on computer vision and pattern recognition*, pp. 4700–4708, 2017.
- [33] M. Sandler, A. G. Howard, M. Zhu, A. Zhmoginov, and L.-C. Chen, "Mobilenetv2: Inverted residuals and linear bottlenecks," *2018 IEEE/CVF Conference on Computer Vision and Pattern Recognition*, pp. 4510–4520, 2018.
- [34] N. Houlsby, A. Giurgiu, S. Jastrzebski, B. Morrone, Q. de Laroussilhe, A. Gesmundo, M. Attariyan, and S. Gelly, "Parameter-efficient transfer learning for nlp," in *International Conference on Machine Learning*, 2019.

- [35] S. Xie, J. Qiu, A. Pasad, L. Du, Q. Qu, and H. Mei, “Hidden state variability of pretrained language models can guide computation reduction for transfer learning,” in *Empirical Methods in Natural Language Processing*, 2022.
- [36] U. Evci, V. Dumoulin, H. Larochelle, and M. C. Mozer, “Head2toe: Utilizing intermediate representations for better transfer learning,” in *International Conference on Machine Learning*, 2022.
- [37] V. Kothapalli, E. Rasromani, and V. Awatramani, “Neural collapse: A review on modelling principles and generalization,” *arXiv preprint arXiv:2206.04041*, 2022.
- [38] “Neural collapse under cross-entropy loss,” *Applied and Computational Harmonic Analysis*, vol. 59, pp. 224–241, 2022. Special Issue on Harmonic Analysis and Machine Learning.
- [39] W. Ji, Y. Lu, Y. Zhang, Z. Deng, and W. J. Su, “An unconstrained layer-peeled perspective on neural collapse,” in *International Conference on Learning Representations*, 2022.
- [40] D. G. Mixon, H. Parshall, and J. Pi, “Neural collapse with unconstrained features,” *arXiv preprint arXiv:2011.11619*, 2020.
- [41] A. Rangamani and A. Banburski-Fahey, “Neural collapse in deep homogeneous classifiers and the role of weight decay,” in *ICASSP 2022-2022 IEEE International Conference on Acoustics, Speech and Signal Processing (ICASSP)*, pp. 4243–4247, IEEE, 2022.
- [42] T. Galanti, A. György, and M. Hutter, “On the role of neural collapse in transfer learning,” in *International Conference on Learning Representations*, 2022.
- [43] L. Hui, M. Belkin, and P. Nakkiran, “Limitations of neural collapse for understanding generalization in deep learning,” *arXiv preprint arXiv:2202.08384*, 2022.
- [44] V. Pappas, “Traces of class/cross-class structure pervade deep learning spectra,” *Journal of Machine Learning Research*, vol. 21, no. 252, pp. 1–64, 2020.
- [45] H. He and W. J. Su, “A law of data separation in deep learning,” *arXiv preprint arXiv:2210.17020*, 2022.
- [46] I. Ben-Shaul and S. Dekel, “Nearest class-center simplification through intermediate layers,” *arXiv preprint arXiv:2201.08924*, 2022.
- [47] L. Xie, Y. Yang, D. Cai, D. Tao, and X. He, “Neural collapse inspired attraction-repulsion-balanced loss for imbalanced learning,” *arXiv preprint arXiv:2204.08735*, 2022.
- [48] Y. Yang, L. Xie, S. Chen, X. Li, Z. Lin, and D. Tao, “Do we really need a learnable classifier at the end of deep neural network?,” *arXiv preprint arXiv:2203.09081*, 2022.
- [49] C. Thrampoulidis, G. R. Kini, V. Vakilian, and T. Behnia, “Imbalance trouble: Revisiting neural-collapse geometry,” *arXiv preprint arXiv:2208.05512*, 2022.
- [50] N. Nayman, A. Golbert, A. Noy, T. Ping, and L. Zelnik-Manor, “Diverse imagenet models transfer better,” *arXiv preprint arXiv:2204.09134*, 2022.
- [51] T. Wang and P. Isola, “Understanding contrastive representation learning through alignment and uniformity on the hypersphere,” in *International Conference on Machine Learning*, pp. 9929–9939, PMLR, 2020.
- [52] H. Azizpour, A. S. Razavian, J. Sullivan, A. Maki, and S. Carlsson, “Factors of transferability for a generic convnet representation,” *IEEE transactions on pattern analysis and machine intelligence*, vol. 38, no. 9, pp. 1790–1802, 2015.
- [53] C. Zhang, S. Bengio, and Y. Singer, “Are all layers created equal?,” *arXiv preprint arXiv:1902.01996*, 2019.
- [54] S. Ioffe and C. Szegedy, “Batch normalization: Accelerating deep network training by reducing internal covariate shift,” *ArXiv*, vol. abs/1502.03167, 2015.
- [55] K. Simonyan and A. Zisserman, “Very deep convolutional networks for large-scale image recognition,” *arXiv preprint arXiv:1409.1556*, 2014.

- [56] Y. LeCun, C. Cortes, and C. Burges, "Mnist handwritten digit database. at&t labs," 2010.
- [57] J. Deng, W. Dong, R. Socher, L.-J. Li, K. Li, and L. Fei-Fei, "Imagenet: A large-scale hierarchical image database," in *2009 IEEE conference on computer vision and pattern recognition*, pp. 248–255, Ieee, 2009.
- [58] H. Xiao, K. Rasul, and R. Vollgraf, "Fashion-mnist: a novel image dataset for benchmarking machine learning algorithms," *ArXiv*, vol. abs/1708.07747, 2017.
- [59] H. He and W. Su, "A law of data separation in deep learning," *ArXiv*, vol. abs/2210.17020, 2022.
- [60] A. Madry, A. Makelov, L. Schmidt, D. Tsipras, and A. Vladu, "Towards deep learning models resistant to adversarial attacks," in *International Conference on Learning Representations*, 2018.
- [61] C. Sun, A. Shrivastava, S. Singh, and A. K. Gupta, "Revisiting unreasonable effectiveness of data in deep learning era," *2017 IEEE International Conference on Computer Vision (ICCV)*, pp. 843–852, 2017.
- [62] F. Utrera, E. Kravitz, N. B. Erichson, R. Khanna, and M. W. Mahoney, "Adversarially-trained deep nets transfer better: Illustration on image classification," in *International Conference on Learning Representations*, 2021.
- [63] Z. Shen, Z. Liu, J. Qin, M. Savvides, and K.-T. Cheng, "Partial is better than all: Revisiting fine-tuning strategy for few-shot learning," in *AAAI*, 2021.
- [64] T. Ridnik, E. Ben-Baruch, A. Noy, and L. Zelnik-Manor, "Imagenet-21k pretraining for the masses," *ArXiv*, vol. abs/2104.10972, 2021.
- [65] K. H. R. Chan, Y. Yu, C. You, H. Qi, J. Wright, and Y. Ma, "Redunet: A white-box deep network from the principle of maximizing rate reduction," *ArXiv*, vol. abs/2105.10446, 2021.
- [66] N. Timor, G. Vardi, and O. Shamir, "Implicit regularization towards rank minimization in relu networks," *ArXiv*, vol. abs/2201.12760, 2022.
- [67] I. Loshchilov and F. Hutter, "SGDR: Stochastic gradient descent with warm restarts," in *International Conference on Learning Representations*, 2017.
- [68] F. Ramzan, M. U. G. Khan, A. Rehmat, S. Iqbal, T. Saba, A. Rehman, and Z. Mehmood, "A deep learning approach for automated diagnosis and multi-class classification of alzheimer's disease stages using resting-state fmri and residual neural networks," *Journal of Medical Systems*, vol. 44, no. 2, 2019.
- [69] J. Ba, J. R. Kiros, and G. E. Hinton, "Layer normalization," *ArXiv*, vol. abs/1607.06450, 2016.

Appendices

The appendices are organized as follows. In Appendix A, we review other metrics that measure feature diversity and discrimination. In Appendix B, we provide experimental details for each figure and each table in the main body of the paper. In Appendix C, we provide extra experiments for the proposed efficient fine-tuning methods in Section 3.3. Finally, in Appendix D, we provide complimentary experimental results for Section 3.1 & Section 3.2.

A Other Metrics for Measuring \mathcal{NC}

Numerical rank of the features \mathbf{H} . The \mathcal{NC}_1 does not directly reveal the dimensionality of the features spanned for each class. Measuring the rank of the features (\mathbf{H}_k) is more suitable. However, the calculations for both \mathcal{NC}_1 and rank are expensive when feature dimension gets too large. Thus, we introduce *numerical rank* [66] as an approximation

$$\widetilde{\text{rank}}(\mathbf{H}) := \frac{1}{K} \sum_{k=1}^K \|\mathbf{H}_k\|_F^2 / \|\mathbf{H}_k\|_2^2,$$

where $\|\cdot\|_F$ represents the Frobenius norm and $\|\cdot\|_2$ represents the Spectral norm. $\widetilde{\text{rank}}(\mathbf{H})$ (*numerical rank*) could be seen as an estimation of the true rank for any matrix. Note that for calculating the Spectral norm, we use the Power Method to find an approximation. The metric is evaluated by averaging over all the classes. It is expected that the smaller $\widetilde{\text{rank}}(\mathbf{H})$ is, the more collapsed the features are to their class means.

Class-distance normalized variance (CDNV) [42]. To alleviate the computational issue of \mathcal{NC}_1 , the *class-distance normalized variance* (CDNV) introduced in [42] provides an alternative metric that is inexpensive to evaluate. Let \mathcal{X} denotes the space of the input data \mathbf{x} and let \mathbf{Q}_k be the distribution over \mathcal{X} conditioned on the class k . For two different classes with \mathbf{Q}_i and \mathbf{Q}_j ($i \neq j$), the CDNV metric can be described by the following equation: $V_{\phi_\theta}(\mathbf{Q}_i, \mathbf{Q}_j) = \frac{\text{Var}_{\phi_\theta}(\mathbf{Q}_i) + \text{Var}_{\phi_\theta}(\mathbf{Q}_j)}{2\|\mu_{\phi_\theta}(\mathbf{Q}_i) - \mu_{\phi_\theta}(\mathbf{Q}_j)\|_2^2}$, where $\mu_{\phi_\theta}(\mathbf{Q}_k) = \mathbb{E}_{\mathbf{x} \sim \mathbf{Q}_k}[\phi_\theta(\mathbf{x})]$ denotes the class-conditional feature mean and $\text{Var}_{\phi_\theta}(\mathbf{Q}_k) = \mathbb{E}_{\mathbf{x} \sim \mathbf{Q}_k}[\|\phi_\theta(\mathbf{x}) - \mu_{\phi_\theta}(\mathbf{Q}_k)\|_2^2]$ denotes the feature variance for the distribution \mathbf{Q}_k . Although the exact expectation is impossible to evaluate, we can approximate them via their empirical means and empirical variances on the given training samples, so that

$$\widehat{V}_{\phi_\theta}(\mathbf{Q}_i, \mathbf{Q}_j) = \frac{\widehat{\text{Var}}_{\phi_\theta}(\mathbf{Q}_i) + \widehat{\text{Var}}_{\phi_\theta}(\mathbf{Q}_j)}{2\|\widehat{\mu}_{\phi_\theta}(\mathbf{Q}_i) - \widehat{\mu}_{\phi_\theta}(\mathbf{Q}_j)\|_2^2}, \quad (5)$$

$$\widehat{\mu}_{\phi_\theta}(\mathbf{Q}_k) = \frac{1}{n_k} \sum_{i=1}^{n_k} \phi_\theta(\mathbf{x}_{k,i}), \quad \widehat{\text{Var}}_{\phi_\theta}(\mathbf{Q}_k) = \frac{1}{n_k} \sum_{i=1}^{n_k} \|\phi_\theta(\mathbf{x}_{k,i}) - \widehat{\mu}_{\phi_\theta}(\mathbf{Q}_k)\|_2^2 \quad (6)$$

To characterize the overall degree of collapse for a model, we can use the average CDNV between all pairwise classes (i.e., $\text{Avg}_{i \neq j}[\widehat{V}_{\phi_\theta}(\mathbf{Q}_i, \mathbf{Q}_j)]$). If a model achieves perfect \mathcal{NC} , obviously we have $\text{Avg}_{i \neq j}[\widehat{V}_{\phi_\theta}(\mathbf{Q}_i, \mathbf{Q}_j)] = 0$. Because the CDNV metric is purely norm-based, computation complexity scales linearly with the feature dimension d , so that it serves as a good surrogate for \mathcal{NC}_1 when the feature dimension d is large.

B Extra Experimental Details

In this section, we include technical details for all the experiments in the main body of the paper. In particular, Appendix B.1 includes all the experimental details for the figures (From Figure 2 to Figure 8), and Appendix B.2 includes all the experimental details for the tables (Table 1 and Table 2).

General training and transfer learning setups. We perform all experiments using single NVIDIA A40 GPUs. Unless otherwise specified, all the pre-training and transfer learning are run for 200 epochs using SGD with a momentum of 0.9, a weight decay of 0.0001 and a dynamical learning rate ranging from 0.1 to 0.0001 controlled by a CosineAnnealing learning rate scheduler as described in [67]. When using ImageNet pre-trained models, we rescale each input image to 224×224 for training, testing and evaluate \mathcal{NC} .

B.1 Technical Detail for the Figures

Experimental details for Figure 2. For the MNIST and FashionMNIST dataset, we train 9-layer MLP models with hidden dimension 784 for 150 epochs. For the Cifar datasets, we train ResNet18 models for 200 epochs. After pre-training, we calculate the layer-wise \mathcal{NC}_1 on the corresponding training datasets and plot the dynamics.

Experimental details for Figure 3. In Figure 3, we pre-train ResNet50 models with different number of projection layers and different loss functions (CE, MSE, SupCon) using Cifar-100 and Mini-ImageNet datasets for 200 epochs. We use n layers MLP projection head to denote adding n linear layers and n ReLU layers in front of the final linear classifier. Then we use the learned model to do transfer learning on Cifar-10. The \mathcal{NC}_1 is then evaluated on the source dataset.

Experimental details for Figure 4. In Figure 4, we pre-train ResNet50 models using different levels of data augmentation and adversarial training. For data augmentation, we consider RandomCrop, RandomHorizontalFlip, ColorJitter and RandomGrayScale. We add an additional augmentation for each level. I.e., for augmentation level 1, we only do the standardization for samples to make the values have mean 0, variance 1 and don't add any data augmentation, for level 2, we add RandomCrop, for level 3, we add RandomCrop + RandomHorizontalFlip, and etc. For adversarial training, we follow the ℓ_∞ norm bounded adversarial training framework in [60] with 5 levels of attack size: $\{\frac{1}{255}, \frac{2}{255}, \frac{3}{255}, \frac{5}{255}, \frac{8}{255}\}$.

Experimental details for Figure 5 and Figure 6. With the same pretraining setup as in Figure 4, we transfer the learned models on 4 different downstream datasets: Cifar-10, FGVS-Aircraft, DTD and Oxford-IIIT-Pet. We note that there are many benchmark datasets that we can potentially use, we choose these 4 datasets because the number of samples for each class is balanced in these datasets, which is the same scenario where \mathcal{NC} is first studied [13]. Additionally, we conduct the same experiments using ImageNet-1k [57] pre-trained ResNet [31], DenseNet [32] and Mobilenet-v2 [33] models.

Experimental details for Figure 8. In Figure 8 (a), we use an ImageNet-1k pre-trained ResNet34 model released online. When conducting the experiments, we first collect the features from each residual block (as shown in Figure 12), then do an adaptive average pooling on the features to

make each channel has only one entry and finally use the resulting features to do the transfer learning and compute \mathcal{NC}_1 . In Figure 8 (b), we use the Vit-B32 model with pre-trained weights released online. For each encoder layer in Vit-B32, the outputs are of size 145 (# of patches + an additional classification token) \times 768 (hidden dimension). For the layer-wise transfer learning experiment, we first do an average pooling on the 145 patches and then train a linear classifier with input dimension 768 on top of each encoder layer.

Experimental details for Figure 11. We choose [5,10,50,100,500,1000,3000,5000] samples from each class of Cifar-10 to form the training dataset and compare the performances of different fine-tuning methods using ResNet18. For layer FT and SCL FT, we fine-tune Block 5 of the network.

B.2 Technical Detail for the Tables

Experimental details for Table 1. For Table 1, we pre-train the standard ResNet18 network on the Cifar-100 dataset under three different choices of loss functions: CE, MSE and SupCon for 200 epochs. Once the model is trained, we only optimize a linear classifier upon the frozen pre-trained models on Cifar-10 dataset for 200 epochs. Both procedures use the cosine learning rate scheduler with initial learning rate 0.1. The \mathcal{NC}_1 is calculated on the source dataset (Cifar100) and the test accuracy is evaluated on the target dataset (Cifar10).

Experimental details for Table 2.

For Table 2, we use a wide variety of experimental setups, including different model architectures, pre-training datasets and downstream datasets. We then compare the performance between linear probing, layer fine-tuning, SCL fine-tuning and full model fine-tuning. For ResNet models, we consider each block as a fine-tuning unit and fine-tune the first block of each layer (e.g., as shown in

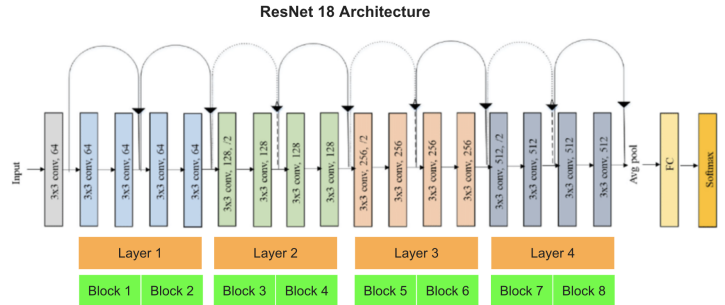


Figure 12: **Fine-tuning unit of ResNet.** Image of ResNet18 from [68]

each layer has 2 blocks, we then fine-tune on the first block of each layer). For Vit-B32 model, we treat each of the 12 encoder layer as a fine-tuning unit. In terms of skip connection, for Vit-B32 model, since the feature dimension from each layer remains constant, the skip connection could be directly applied for the features of the fine-tuned layer and the penultimate layer. However, for ResNet models, the number of channels and the feature dimension change across layers. Therefore, to calculate the skip connection, we first do an adaptive average pooling on the fine-tuned layer features to make each channel has only one entry; then we further do a zero-padding to make the number of channels match with the penultimate layer features. Finally, we apply the skip connection and use the combined features to train the classifier. We note that for the sake of fair comparison, we always let the normalization layers [54, 69] update the running means and variances on the downstream data for all fine-tuning methods we are comparing (linear probing, layer FT, SCL FT and full model FT).

Transfer Acc.										
FT method	Linear Probe	Block 1		Block 3		Block 5		Block 7		Full Model
		Layer FT	SCL FT	Layer FT	SCL FT	Layer FT	SCL FT	Layer FT	SCL FT	
Cifar-10	81.64	91.23	91.76	92.02	92.43	92.12	93.11	93.08	93.65	92.11
Cifar-100	59.75	73.36	75.04	73.87	74.41	74.24	74.35	75.04	75.69	78.65
Aircraft	38.94	55.06	56.86	60.49	61.54	67.36	69.19	68.65	70.24	78.25
DTD	60.16	60.00	62.07	61.70	65.11	66.01	69.84	68.56	71.22	41.38
PET	86.26	86.67	88.14	88.01	89.02	87.90	89.78	86.56	89.18	74.24
Penultimate \mathcal{NC}_1										
Cifar-10	1.82	0.72	0.64	0.51	0.41	0.32	0.27	0.22	0.16	0.08
Cifar-100	22.72	10.50	9.74	7.18	7.16	4.82	3.25	1.60	1.43	0.39
Aircraft	22.50	14.64	12.28	8.30	5.02	5.80	1.78	2.47	1.43	0.75
DTD	4.51	4.05	3.20	2.85	1.82	1.80	0.94	1.10	0.56	1.83
PET	2.32	2.00	1.56	1.49	1.08	1.05	0.63	0.61	0.37	0.38
Percentage of parameters fine-tuned										
	0.23%	0.89%		2.28%		8.43%		33.02%		100%

Table 3: **Transfer learning performance (Top) and penultimate \mathcal{NC}_1 (Bottom) of ResNet18 (pre-trained on Imagenet) on downstream datasets with different fine tuning methods.**

C Extra Experimental Results for Efficient Fine-Tuning in Section 3.3

In Table 2, for the clarity of presentation, we report the maximum transfer performance gained fine-tuning different layers. Here, we report the results for all of the fine-tuned layers in Table 3, Table 4 and Table 5 for ResNet18, ResNet50 and ViT-B32 respectively.

We note that although more collapsed penultimate features almost surely lead to better transferability for fixed feature transfer learning (linear probing), it is not always reliable in the case of model fine-tuning. This is because the more we change model parameters before the linear classifier, the model becomes more prone to remember the data-label relationship in the downstream datasets and hence make the fine-tuned model likely to overfit. Eventually, when the full model is being fine-tuned, we would get a neural collapsed model on the downstream training data but the collapse in this case may not translate to better performances on the test set. Such phenomenon happens especially severely for the datasets with limited number size, as shown in [43].

D Other Complementary Experimental Results

D.1 Additional Results for Section 3.2

In Figure 5, we show that the \mathcal{NC}_1 on Cifar-10 dataset negative correlates with the transfer accuracy on different downstream tasks. Nevertheless, in Figure 13, when we evaluate the relationship between the transfer accuracy and the associated \mathcal{NC}_1 on the same downstream dataset, we cannot find a strong correlation. We conjecture that the reason behind such mismatch is the similar with our analysis in Section 3.1: when the values of \mathcal{NC}_1 get too large, the metric starts to become less meaningful since the increase may come from either an expansion in the feature variance within each class or a loss of discriminative power between classes.

D.2 Additional Results for Section 3.3

Here we show the layer-wise dynamic \mathcal{NC}_1 for the ViT-B32 model in Figure 14. We can observe that the ViT model always has the minimum \mathcal{NC}_1 at the last layers. We note that we use the classification token of each layer to calculate the associate \mathcal{NC}_1 .

Transfer Acc.										
FT method	Linear Probe	Block 1		Block 4		Block 8		Block 14		Full Model
		Layer FT	SCL FT	Layer FT	SCL FT	Layer FT	SCL FT	Layer FT	SCL FT	
Cifar-10	85.33	93.64	93.45	93.54	93.78	94.04	94.94	93.35	94.14	85.51
Cifar-100	65.47	77.82	78.40	77.75	77.76	77.47	78.32	76.44	77.13	78.88
Aircraft	43.23	53.17	55.45	61.18	62.74	70.27	70.72	72.67	74.26	80.77
DTD	68.46	65.96	68.94	66.01	69.84	67.66	72.87	71.81	74.89	38.83
PET	89.26	89.67	90.95	89.92	91.41	89.40	91.69	90.13	91.71	73.24
Penultimate \mathcal{NC}_1										
Cifar-10	1.84	0.63	0.58	0.49	0.40	0.28	0.22	0.15	0.09	0.17
Cifar-100	18.36	7.72	7.24	5.78	5.57	3.22	2.61	1.27	0.84	0.15
Aircraft	20.36	13.87	11.27	9.20	5.01	3.37	1.02	1.27	0.37	0.61
DTD	3.52	3.45	2.64	2.72	1.45	1.68	0.64	0.78	0.51	1.85
PET	1.45	1.39	1.07	1.06	0.76	0.68	0.39	0.32	0.16	0.28
Percentage of parameters fine-tuned										
	0.43%	0.75%		2.04%		6.84%		26.01%		100%

Table 4: Transfer learning performance (Top) and penultimate \mathcal{NC}_1 (Bottom) of ResNet50 (pre-trained on Imagenet) on downstream datasets with different fine tuning methods.

Transfer Acc.										
FT method	Linear Probe	Layer 2		Layer 5		Layer 8		Layer 11		Full Model
		Layer FT	SCL FT	Layer FT	SCL FT	Layer FT	SCL FT	Layer FT	SCL FT	
DTD	73.88	76.54	77.02	75.85	77.18	77.13	77.34	76.12	76.54	76.54
PET	92.23	92.42	92.23	92.67	93.19	92.94	93.13	93.02	93.13	93.02
Aircraft	43.65	57.64	56.50	64.93	62.35	65.83	65.80	62.80	62.32	64.66
Penultimate \mathcal{NC}_1										
DTD	1.99	1.54	1.62	1.21	1.46	1.62	1.33	1.61	1.62	1.11
PET	0.66	0.43	0.50	0.40	0.40	0.44	0.35	0.44	0.36	0.21
Aircraft	17.91	0.21	0.12	0.14	0.11	0.13	0.10	0.11	0.10	0.11
Percentage of parameters fine-tuned										
	0.04%	8.14%		8.14%		8.14%		8.14%		100%

Table 5: Transfer learning performance of Vit-B32 (pretrained on JFT and ImageNet-21k) on downstream datasets with different fine tuning methods.

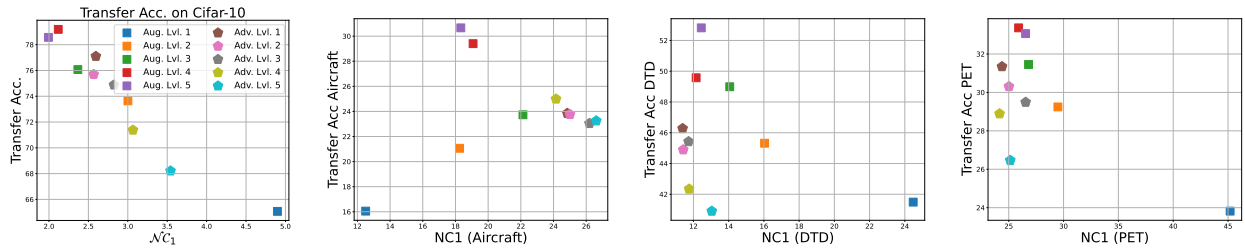


Figure 13: Transfer accuracy on different downstream tasks and \mathcal{NC}_1 . Transfer accuracy and \mathcal{NC}_1 are measured on the same downstream datasets.

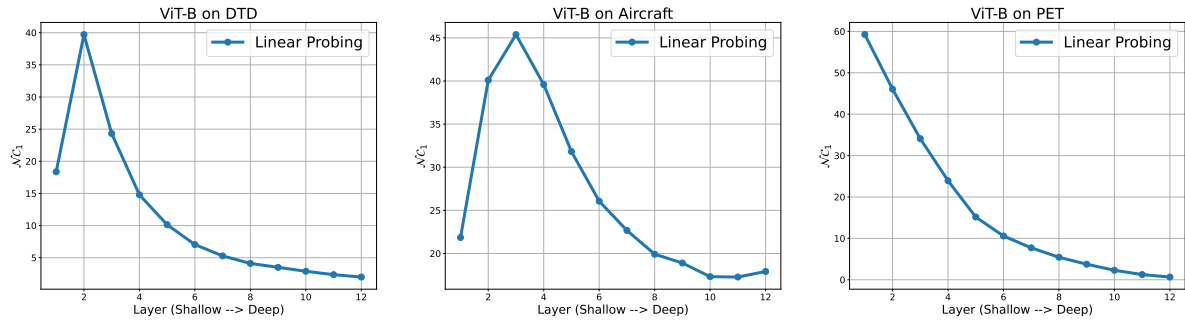


Figure 14: **Layer-wise $\mathcal{N}\mathcal{C}_1$ for ViT-B32 model on various downstream datasets** $\mathcal{N}\mathcal{C}_1$ are measured on the corresponding downstream datasets.